



HAL
open science

New results on the relation between tyre-road longitudinal stiffness and maximum available grip for motor car

Arnaud Andrieux, Pierre Olivier Vandanjon, Régis Lengellé, Christian Chabanon

► To cite this version:

Arnaud Andrieux, Pierre Olivier Vandanjon, Régis Lengellé, Christian Chabanon. New results on the relation between tyre-road longitudinal stiffness and maximum available grip for motor car. *Vehicle System Dynamics*, 2010, 48 (12), pp.1511-1533. 10.1080/00423111003770421 . hal-04801048

HAL Id: hal-04801048

<https://hal.science/hal-04801048v1>

Submitted on 25 Nov 2024

HAL is a multi-disciplinary open access archive for the deposit and dissemination of scientific research documents, whether they are published or not. The documents may come from teaching and research institutions in France or abroad, or from public or private research centers.

L'archive ouverte pluridisciplinaire **HAL**, est destinée au dépôt et à la diffusion de documents scientifiques de niveau recherche, publiés ou non, émanant des établissements d'enseignement et de recherche français ou étrangers, des laboratoires publics ou privés.



Distributed under a Creative Commons Attribution - NonCommercial 4.0 International License

New results on the relation between tire-road longitudinal stiffness and maximum available grip for motor car

A. ANDRIEUX^a, P.O. VANDANJON^{b*}, R. LENGELLE^c and C. CHABANON^a

^a*RENAULT SAS, Guyancourt, 78288 FRANCE;*

^b*Laboratoire Central des Ponts et Chaussées, LCPC, Bouguenais, 44341 FRANCE;*

^c*ICD-M2S FRE CNRS 2848 University of Technology of Troyes, Troyes, 10010 FRANCE*

Tire-road Estimation methods have been the objective of many research programs throughout the world. Most of these methods aim at estimating the friction components such as tire longitudinal slip rate κ and friction coefficient μ in the contact patch area. In order to estimate the maximum available friction coefficient μ_{max} , these methods generally use a probabilistic relationship between the grip obtained for low tire excitations (such as constant speed driving) and the grip obtained for high tire excitations (such as emergency braking maneuver). Confirmation or invalidation of this relationship from experimental results is the purpose of this paper.

Experiments have been carried out on a reference track including several test boards corresponding to a wide textural spectrum. The main advantage of these experiments lies in the use of a vehicle allowing us to accurately build point by point the relationship between κ and μ . This relationship has been determined for different tires, pavement textures.

Finally, the curves obtained are analysed to check the validity of the relationship between the current friction coefficient used by the car during normal driving conditions and μ_{max} .

Keywords: Tire-road friction; Available grip; Longitudinal slip rate; Road texture; Embedded measurement

1. Introduction

Today's vehicles use more and more driver assistance systems and vehicle handling systems : antilock braking system (ABS), electronic stability program (ESP), adaptive and stop-and-go cruise control, downhill speed regulator, advanced automatic driving, etc. From this point of view, embedded tire-road friction estimation is advantageous for improving the driver assistance system efficiency and to provide drivers with an instantaneous warning about the available grip and limits for their possible driving actions.

Due to the importance of tire-road friction, many research programs have been carried out. Two main methods named 'cause based' and 'effect based' have been investigated and developed. 'Cause based' methods [1], [2] attempt to measure external parameters such as pavement texture characteristics [3] or water thickness [4], which directly impact tire-road friction. Due to specific sensors and velocity sensitivity, these methods are quite difficult to implement and are not reliable enough for industrial applications. 'Effect based' methods [5], [6], [7] are more

*Corresponding author. Email : pierre-olivier.vandanjon@lepc.fr, Phone : 33 240845634, Fax : 33 240845993

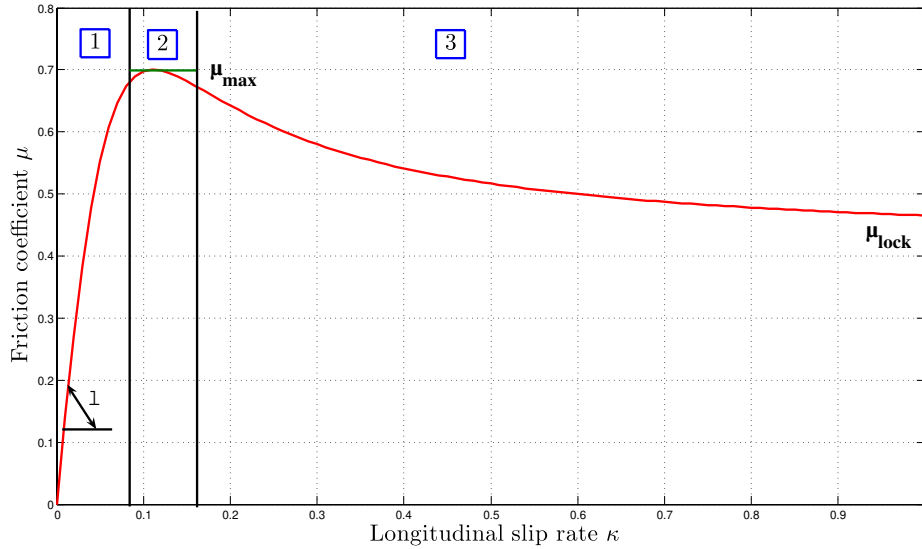


Figure 1. Example of function $\mu = f(\kappa)$ for a wet pavement.

widely used. Their objective is to estimate the friction components such as tire longitudinal slip rate κ and friction coefficient μ in the contact patch area from low or high grip requirement driving conditions. Generally in 'effect based' methods, these estimates are obtained thanks to on board equipment delivering the following signals for each side of the vehicle :

- front angular wheel speed ω_f , corresponding to the driving wheel speed
- rear angular wheel speed ω_r
- effective wheel radii R_f and R_r of front and rear wheels respectively
- front longitudinal traction force F_x
- front normal ground reaction force F_z

These signals are used to compute the longitudinal slip rate κ according to,

$$\begin{aligned} \kappa &= (R_f \omega_f - R_r \omega_r) / R_f \omega_f \text{ if } F_x > 0 \\ \kappa &= (R_r \omega_r - R_f \omega_f) / R_r \omega_r \text{ if } F_x < 0 \end{aligned} \quad (1)$$

and the friction coefficient μ ,

$$\mu = F_x / F_z. \quad (2)$$

The tire-road interaction is represented in the (μ, κ) space which is often used in the literature, see [8], [9], [10] and [11]. Figure 1 shows an example of the variation of the friction coefficient μ as a function of slip κ for a wet pavement. At a given speed and for a given vehicle weight (F_x and F_z are constant), driving conditions correspond to one value of μ . The curve of the figure 1 can be divided into three parts. The first part of the curve shows a quick linear rise corresponding to stable braking. During the second part, the curve reaches a maximum (μ_{max}) corresponding roughly to ABS braking. μ_{max} depends on the micro-texture and macro-texture of the pavement and its lubrication. The third part of the curve shows a smooth

downward slope until a bound (μ_{lock}), corresponding to the grip available during a locked wheels braking with 100% slip, is reached.

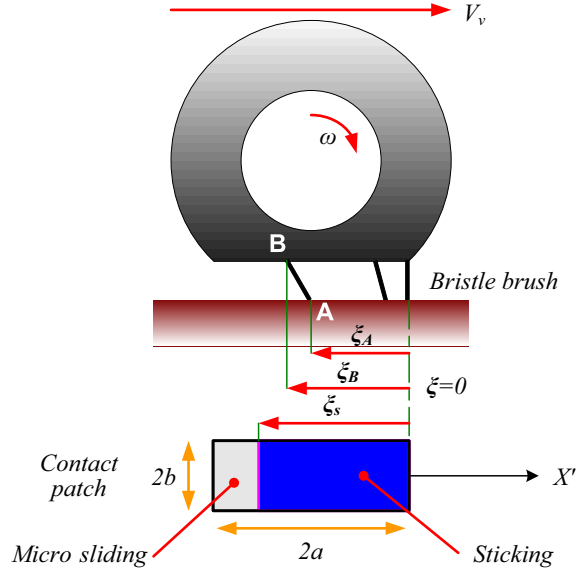


Figure 2. Brush model during driving.

Uchanski [9] proposed an analytic expression of this relation based on the tire-road brush model. Figure 2 shows a representation of this model during acceleration. In the tire-road brush model, a tire is considered as an unstretchable cylinder which can deform under the axle load to provide a contact patch area of $2a$ long and $2b$ wide. Attached to this cylinder are small rubber brush elements showing a longitudinal stiffness k_p . The coordinate of a point in the contact patch is given by its localisation along the ξ axis, which has its zero reference at the beginning of the contact patch and its positive direction pointing towards the rear of the patch. The end of the brush element in contact with the ground is A and its coordinate is ξ_A . The connection between the cylinder and the other end of the brush element is B , its coordinate is ξ_B . The coordinate ξ_s fits with the boundary between the sticking zone and the micro-sliding zone. In the sticking zone, the bristles are not completely stretched and the point A is fixed to the ground. In the micro-sliding zone, the bristles are completely stretched and the A point moves from the ground. The bristles located in the micro-sliding zone use the maximum available grip μ_{max} . Finally the $\mu = f(\kappa)$ is given by :

$$\mu = 3\frac{C}{F_z}\kappa - 3\frac{C^2}{\mu_{max}F_z^2}\kappa^2 + \frac{C^3}{\mu_{max}^2F_z^3}\kappa^3 \quad (3)$$

where $C = \frac{4}{3}a^2bk_p$ is a constant in relation to the contact patch size and the longitudinal stiffness of the bristle tire gum.

In order to estimate the maximum available friction coefficient μ_{max} , 'effect based' methods generally use a probabilistic relationship between the grip obtained for low tire excitations (such as constant speed driving) and the grip obtained for high tire excitations (such as emergency braking maneuver). This relation assumes that the slope of the $\mu = f(\kappa)$ curve in the linear part of the curve contains information about the maximum available grip : the greater the value of μ_{max} , the

greater the slope λ . The derivation of expression (3) contains information about μ_{max} and confirms these assumptions (see (4)). A variation of μ_{max} involves a variation of λ .

$$\frac{\partial \mu}{\partial \kappa} = 3 \frac{C}{F_z} - 6 \frac{C^2}{\mu_{max} F_z^2} \kappa + 3 \frac{C^3}{\mu_{max}^2 F_z^3} \kappa^2 \quad (4)$$

From an experimental point of view, the literature does not offer many results concerning the influence of μ_{max} on the slope λ . Gustafson [5, 12] produced the main experimental result showing two distinctive slopes λ between a dry and a snow covered pavement. Many researchers used Gustafsson's results as a starting point [9, 13, 14]. This approach requires big and expensive trial means. This explains the lack of experiments. Another approach can be found in the Michelin patent [15] which describes an invariant relationship between coordinates of the top of the $\mu = f(\kappa)$ curve and coordinates of a point belonging to this linear part (see (5)). This paper aims to compare these results to experimental data in order to confirm or invalidate these approaches.

$$\frac{\frac{\mu_{max}}{\kappa|_{\mu_{max}}}}{\frac{\mu\left(\kappa|_{\mu_{max}}/2\right)}{\kappa|_{\mu_{max}}/2}} = Inv = 0,58 \quad (5)$$

2. Methods of measurement

To study the relationship between μ_{max} and λ , our goal is to acquire (μ, κ) accurate coordinates for different pavements and different tires. Usually, the relation $\mu = f(\kappa)$ is computed with measurements coming from dedicated test benches called rolling machines or from dedicated vehicles including a measuring wheel. The first and second paragraph of this section aims at explaining why these test benches and dedicated vehicles are hardly appropriate to our objectives. Another way to calculate the relation $\mu = f(\kappa)$ is to store data during an emergency frontal braking. The third paragraph of this section shows the metrological difficulties of such a system. Finally, our trial means, based on controlled deceleration of the vehicle, are described.

2.1. Specific test benches

To easily determine the relation $\mu = f(\kappa)$, tire and car manufacturers use specific test benches called rolling machines. These machines make it possible to subject a tire to specific conditions : the tire can be loaded, swung, accelerated and inflated to a specific pressure. There are three types of rolling machines :

- Internal steering wheel rolling machines : tires are inside a large and rigid steering wheel,
- external steering wheel rolling machines : tires are outside a large and rigid steering wheel,
- flat-track rolling machines : tires are on an horizontal metallic belt, see figure 3.

Despite their good performances, rolling machines, are not entirely suitable for varying the pavement texture and pavement lubrication. Only flat-track rolling machines can change the micro-texture of the abrasive paper of its rolling belt. But any rolling machine can add water in the contact patch area. This parameter variation is essential to determine the impact of pavement characteristics on tire grip. As a conclusion, rolling machines are well suited to determine tire characteristics but not to determine tire-road mechanisms. On the contrary, experiments based on vehicle satisfy these constraints.

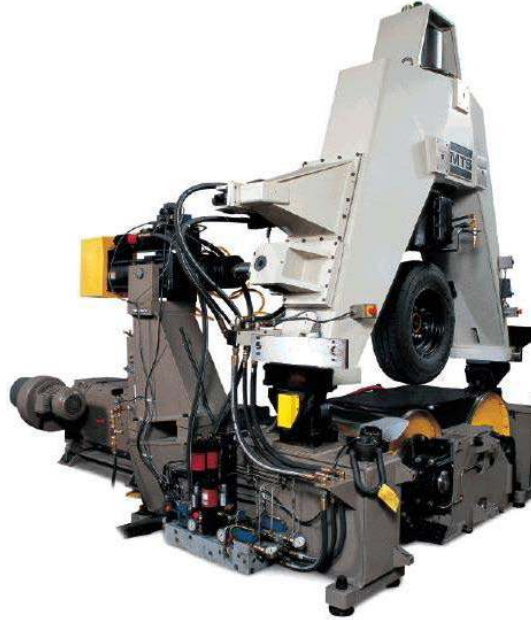


Figure 3. Exemple of a test bench for tire behavior study : MTS Flat-trac.

2.2. *Five wheels test vehicles*

To take into account the influence of pavement texture and pavement lubrication on tire road friction, specific vehicles have been developed. These vehicles are usually 4 wheels tank trucks which are equipped with an extra wheel for tire/road friction measurement and a pavement lubrication system. The added wheel is either inside the vehicle or on a pulled trailer. In the following, these vehicles are called 'five wheels test vehicles'.

There are roughly two types of devices : devices for measuring the conventional skid resistance which are often managed by road authorities and devices for research activity.

2.2.1. *Measuring devices for conventional skid resistance*

In order to manage the maintenance of national road networks, authorities need specific measuring devices to control quickly and effectively the grip offered by the road. If we focus on the longitudinal friction coefficient, some equipments are enable to measure the skid resistance within the respect of operating constraints. In Europe the main ones are : the Adhera 2 in France, the BV 12 in Sweden and the RoadStar in Austria [16]. The figure 4 shows the Adhera 2.



Figure 4. Example of 'five wheels test vehicles', ADHERA 2.

For example, characteristics of Adhera 2 are given. This equipment is designed to measure the Longitudinal Friction Coefficient (LFC). The measurement is done by a sensor wheel subjected to a constant vertical load (250 daN) which is pulled at a constant speed by a tank truck which spreads a 1 mm water layer on pavement. During the measurement, the rotation of the wheel is prevented along a distance of 20 m . Then the LCF is deduced from the measurement of the average torque ensuring balance with the friction torque exerted by the pavement on the tire.

Generally, such vehicles measure a single point on the curve $\mu = f(\kappa)$. For example, tests with Adhera 2 are conducted locked wheel. This constrain implies that this device delivers only the value of the friction when the slip rate is 100%. Moreover, these devices are equipped with a standard tire that is not representative of actual tires used on a passenger car. For example, Adhera 2 is equipped with the PIARC tire which is a smooth and narrow tire [17].

In short, these standardized test devices are relevant to monitor the quality of a pavement but do not inform us about the relationship between stiffness and maximum available friction coefficient μ_{max} , for a classical vehicle.

2.2.2. Measuring devices for research activities

Besides devices for measuring the conventional skid resistance, some research equipments have been developed to measure the entire curve $\mu = f(\kappa)$. There are the Michelin vehicle C 35, the trailer Dynatest and the Adhera Research [18]. The Adhera Research has the same architecture as the Adhera 2 previously presented. The control of the braking procedure and the data processing is more sophisticated than for Adhera 2. It enable to measure a longitudinal friction coefficient with a slip ratio ranging from 0% to 100% (locked wheel) [19].

While performing, these devices are rare, expensive, difficult to carry out on a test track. They give a global view of the curve $\mu = f(\kappa)$ and are not appropriate to our purpose which is to zoom on the beginning of the curve, i.e. to study the grip at low solicitation. Moreover, the behaviour of a measuring wheel is different from the one of a wheel in a real vehicle. So, it will be difficult to extrapolate these results to a real car.

2.3. Emergency frontal braking

To take into account the influence of pavement texture and pavement lubrication on the $\mu = f(\kappa)$ curve, for a given tire, trial vehicles seem to be a good solution [16]. In order to obtain the full curve, the pilot makes a frontal emergency braking

without anti-lock braking system. On such vehicles, the longitudinal slip rate κ is calculated using an optical velocity sensor (like Correvit), used as a reference, and high resolution encoders on braking wheels and the longitudinal friction coefficient μ is computed using the acceleration signal from an inertial system injected in a bicycle model. On some trial vehicles, the friction coefficient can be provided by a dynamometric wheel. Figure 5 shows the evolution of μ as a function of κ and their evolution as a function of time for an emergency braking from an initial vehicle speed of 90 km/h .

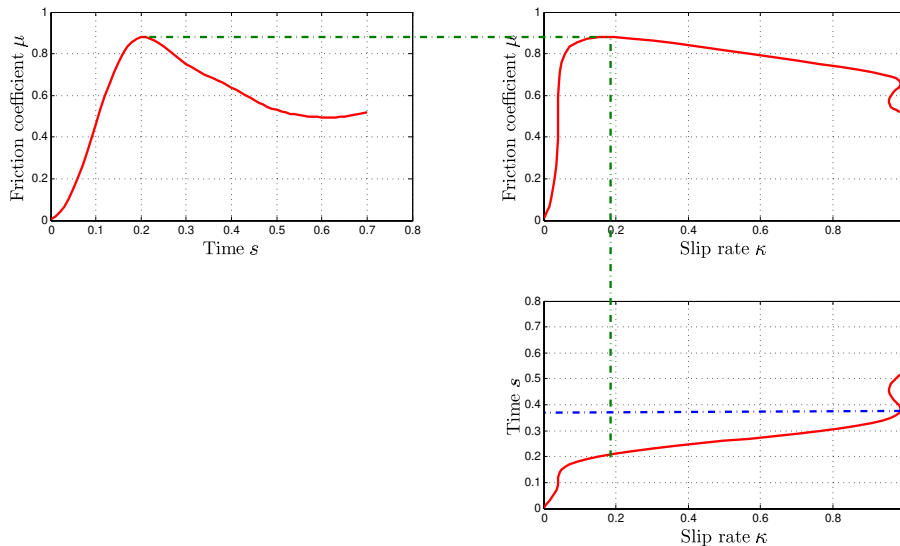


Figure 5. The central subfigure represents the evolution of μ as a function of κ for an emergency braking on a wet pavement. The left subfigure and the lower subfigure represent respectively the evolution of μ as a function of time and the evolution of κ as a function of time.

As shown on figure 5, the time to reach μ_{max} is very small (about 0.2 s) and the time to reach 100% of the slip rate and to lock braking wheels is also very small (about 0.2 s). Due to the rapidity of the mechanisms, it is quite a real challenge to characterize emergency frontal braking metrologically. Indeed, a record of 0.2 s , using for example a sampling frequency of 100 Hz leads to only 20 couples of (μ, κ) coordinates. Moreover, an emergency braking corresponds to a succession of transitory mechanisms of tire-road interaction (shearing of the pieces of gum, load transfer, rise of temperature, etc). Consequently these 20 points are very noisy and do not allow us to study of the variation of the slope λ .

2.4. Controlled deceleration

The proposed solution is braking with controlled deceleration. This method takes advantages from all the techniques previously detailed. The ability to control the vehicle deceleration provides the stability observed with a rolling machine. In addition the use of a trial vehicle allows to take into account the influence of pavement texture and pavement lubrication with an actual tire of passenger car. The vehicle is a classical car : this means that the measured friction is the one required by a car and not an approximation obtained with an artificial device. In addition, this procedure is easy to carry out on a test track.

2.4.1. Theoretical analysis

Our trial vehicle is equipped with a modified braking system that allows it to achieve pure frontal braking by disabling the braking distribution and taking the rear brakes out of service. A controlled pump generates the required pressure on front brakes. Pressures of front brakes are measured and forwarded to the pump regulator. In practical terms, once the vehicle runs at 90 km/h , a pressure step command is sent to the braking system. After the load transfer, a stabilized braking associated with a stabilized deceleration is observed for several seconds. This steady state allows a very accurate measurement of slip rate κ and friction coefficient μ for a specific tire operating point on a real pavement showing a determined level of lubrication.

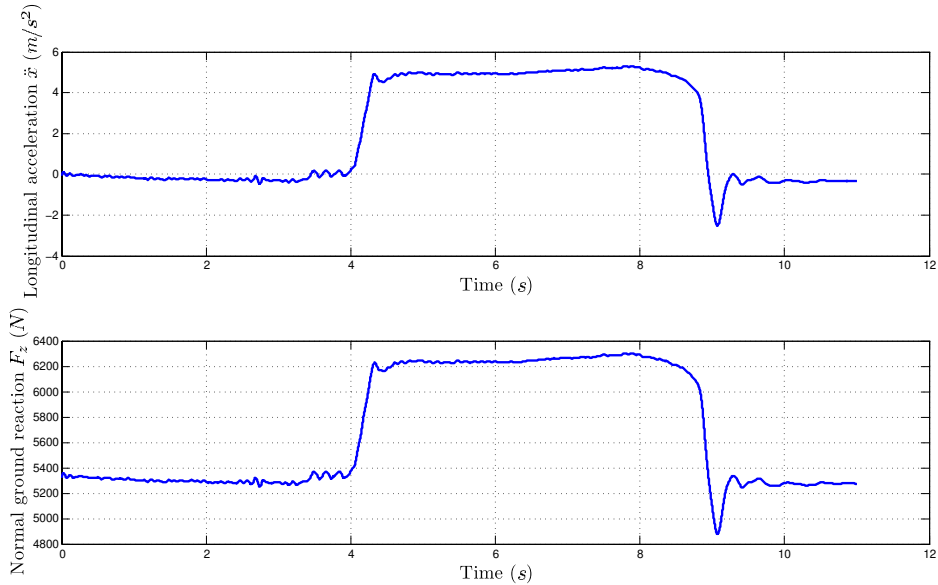


Figure 6. Illustration of the stability of our measurement method. The upper subfigure represents the evolution of \ddot{x} as a function of time and the lower subfigure represents the evolution of F_z as a function of time for a controlled deceleration braking.

Figure 6 shows records of the evolution of the longitudinal acceleration \ddot{x} of the center of gravity of the vehicle and the evolution of the normal ground reaction force F_z as a function of time from our trial vehicle for a controlled deceleration braking. On both curves, the level \ddot{x} and F_z is relatively constant and can be maintained for several seconds ($\approx 3 \text{ s}$). During the braking, only very small and smooth variations can be observed showing that the variations of load transfer can be neglected during braking. These characteristics illustrate the great stability of our measurement method.

We now show the stable state of the vehicle during a braking maneuver using a converse Lyapunov theorem. For the sake of clarity, stability is studied using a simplified model. In the case of a more complex model, the stability has been verified numerically. Figure 7 illustrates our simplified model based on the torque balance at wheel-road contact :

$$J\dot{\omega} = R_{eff} \times \mu(\kappa)F_z - T_B \quad (6)$$

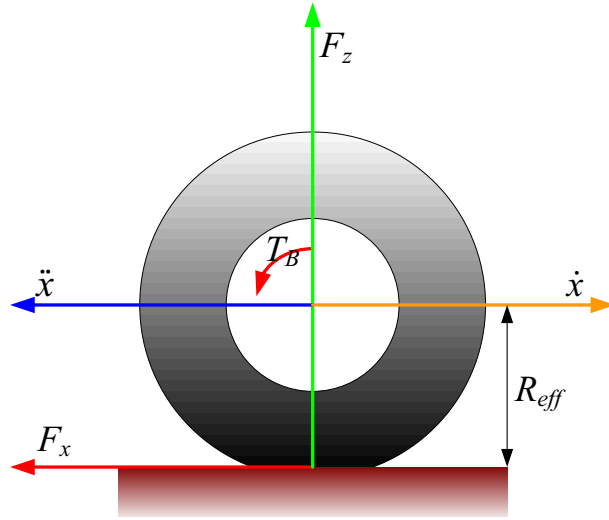


Figure 7. Torque balance at wheel-road contact.

with :

- J : the main inertia of the wheel.
- T_B : the braking torque which is constant.
- R_{eff} : the effective radius.
- F_z : the reaction of the road which supports the wheel. It is supposed that the load transfer is stabilized. Therefore, F_z is assumed constant.
- ω (resp. $\dot{\omega}$) : the angular velocity (resp. acceleration) of the wheel.

By assuming that the braking process is the same for the front right wheel and for the front left wheel (rear brakes are disconnected), the equation of the movement for the vehicle along the longitudinal axis is :

$$M\ddot{x} = -2\mu(\kappa)F_z \quad (7)$$

with :

- M : the mass of the vehicle.
- x, \dot{x}, \ddot{x} : the longitudinal position, speed and acceleration of the center of gravity of the vehicle.

Our objective is to prove that the braking process is stabilized around a constant slip rate when a suitable constant braking torque is applied. Before, remember the definition of κ :

$$\kappa = \frac{\dot{x} - R_{eff}\omega}{\dot{x}}$$

Using 7 and 6, the derivative of κ is given by :

$$\dot{\kappa} = \frac{1}{\dot{x}} \left(\frac{R_{eff}T_B}{J} + \mu(\kappa)F_z \left(-\frac{R_{eff}^2}{J} - \frac{2(1-\kappa)}{M} \right) \right) \quad (8)$$

The stationary slip κ^* is obtained when equation 8 is set to zero.

$$\mu(\kappa^*)F_z \left(\frac{R_{eff}^2}{J} + \frac{2(1 - \kappa^*)}{M} \right) = \frac{R_{eff}T_B}{J} \quad (9)$$

Considering the function $\mu(\kappa)$, illustrated on figure 1, this last equation has :

- no root if the braking torque is too high,
- two roots if μ is included between μ_{max} and μ_{lock} . In the following, it will be demonstrated that one of these two solutions is unstable,
- one root if μ is smaller than μ_{lock} .

Let us now suppose that the braking torque is small enough to get a friction μ below μ_{max} . This is coherent with our experimental procedure.

Now, the stability of the ordinary differential equations 8 is studied around the equilibrium point κ^* . For this purpose, $\tilde{\kappa} = \kappa - \kappa^*$ is introduced.

According to equation 8,

$$\dot{\tilde{\kappa}} = \frac{1}{\dot{x}} f(\tilde{\kappa} + \kappa^*) \quad (10)$$

where f summarizes the part of the equation which varies only with κ . This equation is linearized :

$$\dot{\tilde{\kappa}} = \frac{1}{\dot{x}} \left(f(\kappa^*) + \frac{\partial f(\kappa^*)}{\partial \kappa} \tilde{\kappa} + o(\tilde{\kappa}) \right) \quad (11)$$

with $\lim_{\tilde{\kappa} \rightarrow 0} \frac{o(\tilde{\kappa})}{\tilde{\kappa}} = 0$.

By definition, $f(\kappa^*) = 0$, the linearized system is :

$$\dot{\tilde{\kappa}} = \frac{1}{\dot{x}} \frac{\partial f(\kappa^*)}{\partial \kappa} \tilde{\kappa} \quad (12)$$

According to the theorem 4.15 of the book [20], and under the assumption that the function $\mu(\kappa)$ is smooth enough, κ^* is an exponentially stable equilibrium point for the nonlinear system 8 if, and only if, zero is an exponentially stable equilibrium point for the linear system 12.

The longitudinal speed \dot{x} of the vehicle varies from V_{max} to V_{min} during the braking maneuver. For our experiments, $V_{max} = 25$ m/s. Furthermore, the computation of the slip rate is stopped when $V_{min} \approx 17$ m/s. Thus, the linear system 12 is stable if, and only if :

$$\frac{\partial f(\kappa^*)}{\partial \kappa} < 0 \quad (13)$$

Based on equation 8, the derivative of f is calculated :

$$\frac{\partial f(\kappa^*)}{\partial \kappa} = \left(\frac{\partial \mu(\kappa^*)}{\partial \kappa} F_z \left(-\frac{R_{eff}^2}{J} - \frac{2(1 - \kappa^*)}{M} \right) + 2\mu(\kappa^*) \frac{F_z}{M} \right) \quad (14)$$

As $F_z > 0$, the stability condition 13 becomes :

$$\frac{\partial \mu(\kappa^*)}{\partial \kappa} \left(\frac{R_{eff}^2}{J} + \frac{2(1 - \kappa^*)}{M} \right) > \frac{2\mu(\kappa^*)}{M} \quad (15)$$

Considering numerical values : $R_{eff} \approx 0.3 \text{ m}$, $M \approx 1500 \text{ kg}$, $\kappa \in [0, 0.15]$, $\mu \in [0, 1.5]$, $J \approx 1 \text{ kg.m}^2$, this last condition can be practically approximated by the simplified condition :

$$\frac{\partial \mu(\kappa^*)}{\partial \kappa} > 0 \quad (16)$$

Considering the shape of the function $\mu(\kappa)$ (see figure 2), the stability is ensured if and only if the level of the braking torque corresponds to a friction coefficient below to μ_{max} . For this level, there exists a stable slip rate below to the optimal slip rate corresponding to μ_{max} . The derivative of the $\mu(\kappa)$ curve is positive for this slip rate.

Our experimental procedure was carried out in order to ensure stability.

2.4.2. Trial means

- The trial vehicle : the vehicle used during our trials is a sedan. It is a front wheel drive car equipped with a V6 engine coupled with a 5-speed automatic gear box. Ground link is realized by a pseudo Mac-Pherson front axle and a 'H shape' rear axle. The vehicle weight is 1770 kg.
- Sensors : laboratory sensors with high sensitivity are embedded on the trial vehicle. Measured signals are recorded at 1 kHz thanks to a National Instrument acquisition system. Table 1 describes sensors and figure 8 shows the localisation of these sensors on the trial vehicle.
- The track : during our trials, we used the Reference and Road Experiment Track of the *French Public Works Research Laboratory* at Nantes. This track has the particularity to grouping together 17 pavements representing all scales of micro and macro-texture. The measurement zone of the track includes a number of test boards, ranging from 100 to 250 m in length and 2 m wide. Some of these boards feature 'extreme' textural characteristics, i.e. : a smooth resin finish, a 2/4 mm surface dressing, and a 0/12 mm surface dressing. Other test boards are representative of actual wearing course laid on the French highway network (0/10 mm ultra thin asphalt concrete, 0/6 mm very thin asphalt concrete, and high performance asphalt concrete). A mobile sprinkling system enables the wetting of the various road sections. Figure 9 shows an aerial view of the experiment track.

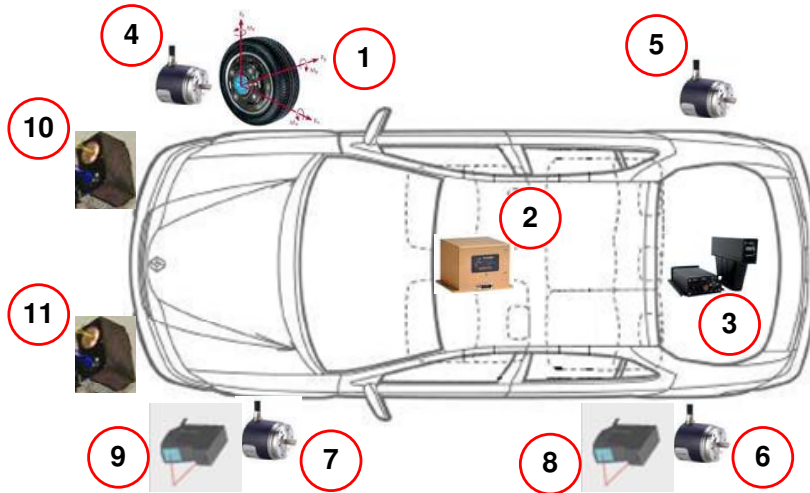


Figure 8. Localisation of sensors embedded on the trial vehicle.

Table 1. Sensors embedded on the trial vehicle

Sensor	N°	Function	Accuracy
Kistler <i>S625</i>	1	Dynamometric wheel to measure forces and torques in the contact patch area.	Full scale linearity 0.39%
Crossbow <i>VG700AA</i>	2	Inertial system to measure X, Y, Z accelerations and <i>Rolling, Pitching, Yaw</i> angular velocities.	$\pm 1\%$
Datron <i>S400</i>	3	Bi-axial Correvit to measure reference vehicle speed.	0.1%
Ivo <i>G0355</i>	4 to 7	Angular encoder to measure wheel speed.	10000 points per revolution
Keyence <i>LK - G157</i>	8 to 9	Laser telemeter to measure tire radius variations.	Full scale linearity 0.05%
Aquasens	10 to 11	Optical sensor to measure water thickness in front of tires.	$\pm 0.1 \text{ mm}$

Figure 9. Reference and Road Experiment Track of the *French Public Works Research Laboratory*.

3. Experimental procedure

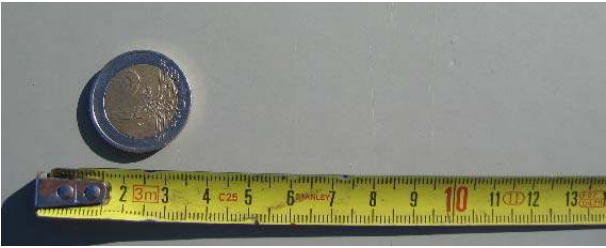




To scan a large range of tire-road friction conditions, the experimental procedure is very important and requires many precautions in its implementation. Factors to be considered are :

- 5 pavements presenting conventional friction coefficient μ ranging from 0.1 to 1.2 with different micro-textures and macro-textures (see table 2).
- 2 types of tires : summer and winter (see table 3).
- 2 tire manufacturers : *A* and *B* (see table 3).
- 2 weakening levels : new and worn (see table 3).
- A fixed amount of water (In fact, surfaces are wetted for 10 minutes, i.e. : each surface receives the same amount of water. For information, this amount of water represents a water thickness of 0.4 *mm* on a traditional pavement).

The combination of these variables gives 40 cases of tire-road friction. To obtain a point by point plot of the $\mu = f(\kappa)$ curves, each case includes 12 brakings with increasing deceleration, 5 random recurrences for two distinct brakings, 1 ABS braking, 1 locked wheels braking and finally 1 braking on a dry surface to measure the tire's vertical stiffness. So we obtained approximately 25 brakings for one modality and consequently 1000 brakings during the whole trial campaign.

Two precautions were taken to perform these experiments. Prior to trials, all tires were run in 1000 *km* in order to take off the silica layer found on new tires and to have a good cylindrical shape for worn tires. During the trials, the tire manufacturer's instructions concerning tire temperature were met : winter tires were used under 7°C and summer tires were used above 11°C.



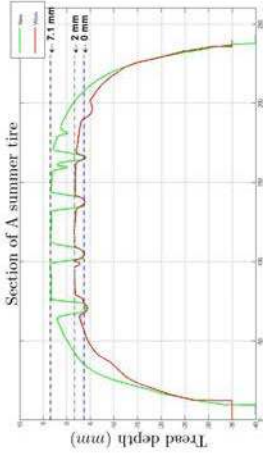


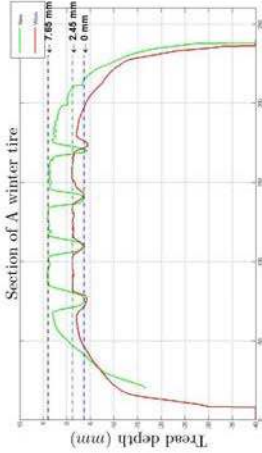


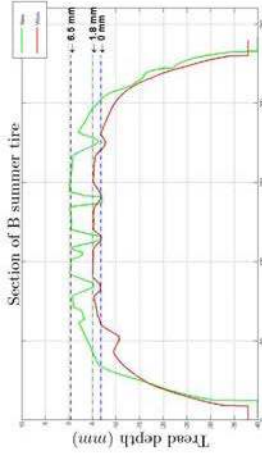


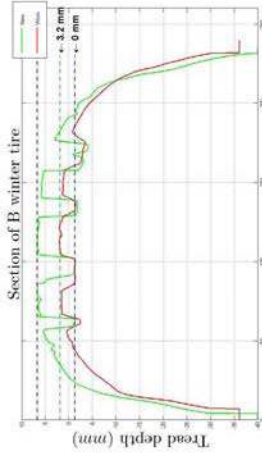
Table 2. pavement properties

Pavement	Name and description
	<p>Epoxy board: Pavement manufactured in epoxy resin. This board is used for very low grip conditions. When this board is wet, its behavior is close to ice. CFL40^a = 0.1 and PTE^b = 0.15.</p>
	<p>Painted board: Soft bituminous concrete painted with pedestrian crossing paint. CFL40= 0.50 and PTE= 0.50.</p>
	<p>Porous board: Porous asphalt 0/6. This surface covering 5% of the French national network is used where it frequently rains. CFL40= 0.67 and PTE= 0.88.</p>
	<p>BBSG board: Medium coarse asphalt (BBSG0/10). This surface is the most widely used on the French national network ($\approx 40\%$). CFL40= 0.71 and PTE= 0.62.</p>
	<p>Colgrip board: Pavement manufactured with a bituminous binder (bitumen and epoxy) and very hard aggregate (refractory calcining bauxite aggregate bounded between 1mm and 3mm). This surface is used for very high grip conditions and in particular in dangerous area. CFL40= 0.93 and PTE= 1.54.</p>

^aCFL40 is the Longitudinal Friction Coefficient provided by a conventional measuring device named *ADHERA* using a slick tire *AIPCR*, locked wheel, 1 mm water thickness, 40 km/h and 250 daN load. (*AIPCR* = *International Association For Road Congress*).

^bPTE is the Equivalent Texture Depth provided by a conventional measuring device named *Rugolaser*.

Table 3. Tires description.

Manufacturer	Type	New tire	Worn tire	Weakening level	Vertical stiffness (N/m)
A	Summer				226.67 (new) 238.56 (worn)
					240.46 (new) 245.49 (worn)
	Winter				236.12 (new) 239.19 (worn)
					232.81 (new) 231.67 (worn)

4. Experimental results

This section presents the experimental results obtained with the means at our disposal for the trial. In a first subsection, a typical $\mu = f(\kappa)$ curve is described. The second subsection deals with the influence of pavement on the shape of $\mu = f(\kappa)$ curve. The third subsection presents the influence of tire on the shape of $\mu = f(\kappa)$ curve. Finally a study of the slope variation of $\mu = f(\kappa)$ curves is proposed.

Remark 1: Figures on table 3 show different notch rates in tire tread. Winter tires are characterized by a high notch rate and a lot of gum blades in order to break the water and snow layers on a pavement and to keep it well drained. This design aims at improving indentation mechanism [21]. Summer tires present a medium notch rate and a few strips in order to maximize the gum surface in contact with the pavement. This design is used to favor adhesion mechanism. Winter tires and summer tires are very different. Nevertheless, their vertical stiffness is similar for a given pressure.

4.1. Point by point representation of $\mu = f(\kappa)$ curves

Figure 10 represents the $\mu = f(\kappa)$ curve for a B new winter tire on the Porous board. This curve is built point by point, each point corresponding to a braking. As expected, the quick linear rise and the beginning of the inflexion to reach the maximum available grip (μ_{max}) can be observed. The repetition series for a low deceleration braking (in diamonds) and for a middle deceleration braking (in squares) are represented on this figure. The relative closeness of these repetition points shows the very good measurements quality and repetitiveness of our method.

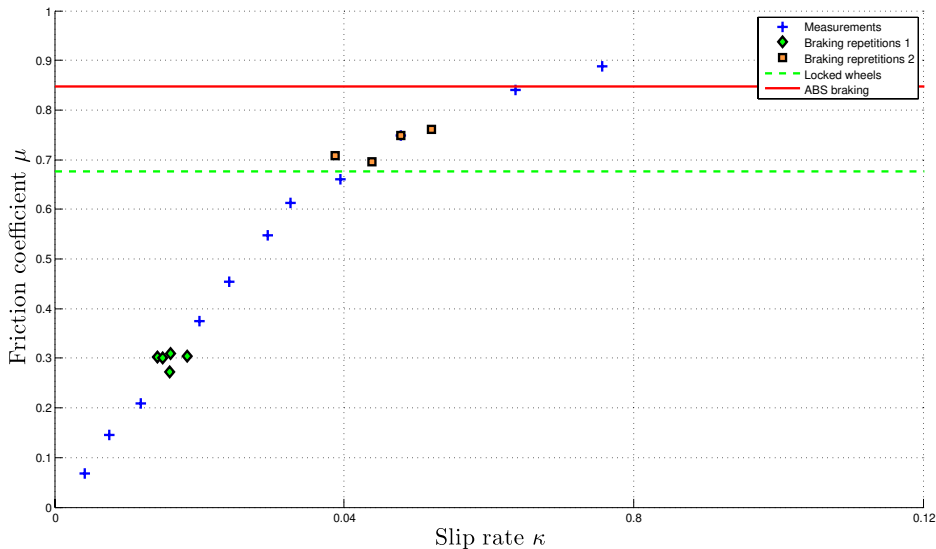


Figure 10. $\mu = f(\kappa)$ for B new winter tire on the Porous board.

This very reliable measurement method allows us to analyse the variation of the slope λ of the curve $\mu = f(\kappa)$. In the literature, the slope λ is also named 'longitudinal stiffness' of the tire/pavement couple. Above the $\mu = f(\kappa)$ curve, the friction coefficient values for an ABS braking (solid line) and a locked wheels

braking (dash line) are plotted. The friction coefficient value obtained for the locked wheels braking is obtained for a 100% slip rate. This value ($\mu_{lock} = 0.67$) is not very high compared with the maximum friction coefficient value reached ($\mu_{max} = 0.89$). This fall of performance results from the tire temperature increase during locked wheels braking which highly impacts the tire grip. The friction coefficient obtained for the ABS braking ($\mu_{ABS} = 0.84$) is slightly smaller than the maximum friction coefficient value ($\mu_{max} = 0.89$). This difference results from the ABS regulation which controls the braking pressure in order to keep the wheel slip around an operating point providing an average grip close to the maximum available grip. The shape of the curve depicted in figure 10 and the scattering of these measuring points are representative of all curves obtained whatever the tire/pavement couple tested.

4.2. Pavement effect

This subsection aims to bring a first summary of the test findings. The $\mu = f(\kappa)$ curves for all pavements are plotted for a given tire. This representation can be called 'pavement effect'. To allow an easy comparison of results, every graph is plotted using the same scale. The curves presented are obtained using inertial system but comparable results are obtained using a dynamometric wheel. This subsection is dedicated to the study of the quick linear rise section of $\mu = f(\kappa)$ curves. Figure 11 shows the pavement effect representation for B new and worn summer tires. This figure can be compared with figure 12 showing the pavement effect representation for B new and worn winter tires.

The observation of maximum friction coefficient values, μ_{max} , of figures 11 and 12 provides the ranking of pavements as a function of their grip for a given tire. For all tires the same ranking is observed and is given by :

- 1st : Colgrip board.
- 2nd : BBSG board.
- 3rd : Porous board.
- 4th : Painted board.
- 5th : Epoxy board.

This ranking shows the very good performances of the Colgrip board always associated with the same maximum friction coefficient value ($\mu_{max} = 1.22$) for all tires. Thus, the Colgrip board can correct bad performance of a worn tire. BBSG board and Porous board are very close so these two pavements cannot always be distinguished. This ranking is in accordance with our a priori knowledge of these surfaces.

The small variations of maximum friction coefficient values μ_{max} will be discussed in the next subsection dedicated to the 'tire effect'.

Figures 11 and 12 exhibit the great difficulty of linking the longitudinal stiffness to the maximum friction coefficient in order to provide an estimate of it. In the following, these figures are interpreted from low slip rates to extreme slip conditions. These curves can be divided into two parts.

- (1) At low slip rates, all the curves are merged i.e. : all the curves $\mu = f(\kappa)$ seem to present the same longitudinal stiffness for a given tire although the maximum available grip significantly differs from one pavement to another.
- (2) When the solicitation increases, an inflexion point is reached. From this inflexion point the curves can be separated : the higher the longitudinal

stiffness, the higher the braking power required to reach the inflexion point. For example, on the lower part of figure 11, the inflexion is located at 90% of the maximum available grip. On the upper part of figure 12, the inflexion is located at 75% of the maximum available grip.

These considerations demonstrate that it will be very difficult, maybe impossible, to estimate the maximum available grip knowing the longitudinal stiffness.

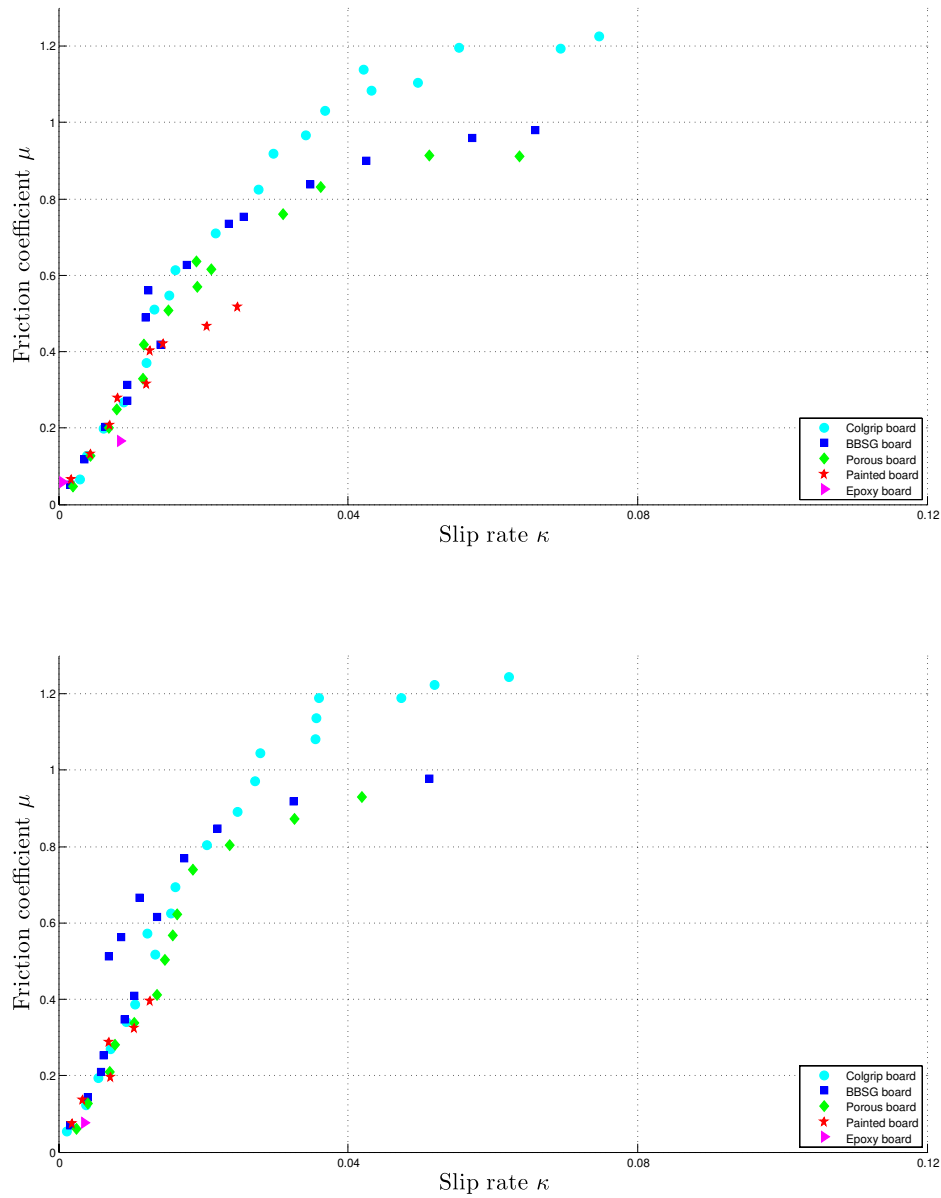


Figure 11. $\mu = f(\kappa)$ for B new (upper subfigure) and worn (lower subfigure) summer tire.

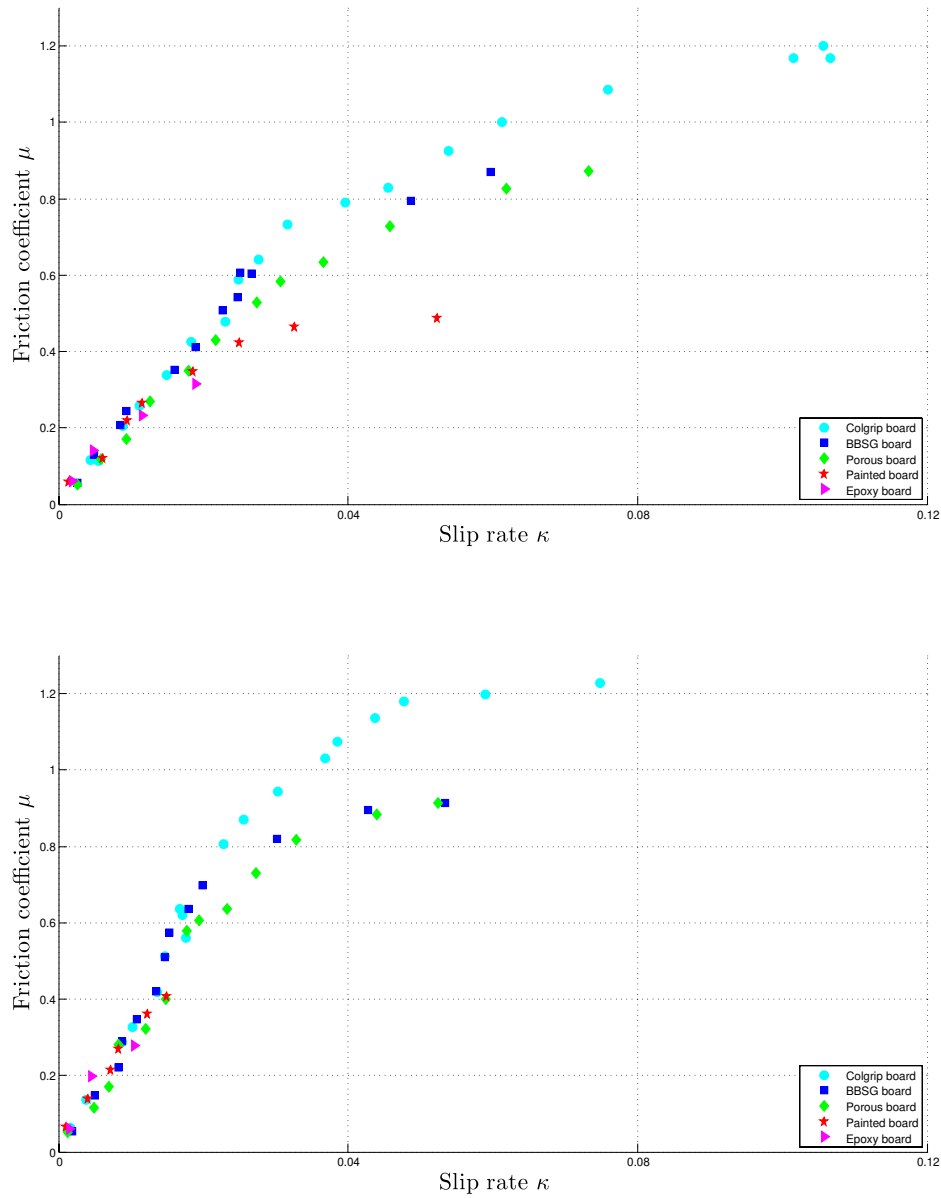


Figure 12. $\mu = f(\kappa)$ for B new (upper subfigure) and worn (lower subfigure) winter tire.

4.3. Tire effect

In this subsection, the $\mu = f(\kappa)$ curves, for all tires, have been plotted for a given pavement. This representation allows us to consider the 'tire effect'. As for previous results, every graph is plotted using the same scale. Here again, the curves presented are obtained using an inertial system but similar results are obtained with a dynamometric wheel. This subsection is also dedicated to the study of the quick linear rise section of $\mu = f(\kappa)$ curves. Figure 13 shows the tire effect for the Colgrip board (upper subfigure) and the BBSG board (lower subfigure). This figure can be compared with figure 14 showing the tire effect for the Porous board (upper subfigure) and the Painted board (lower subfigure). Results of the Epoxy

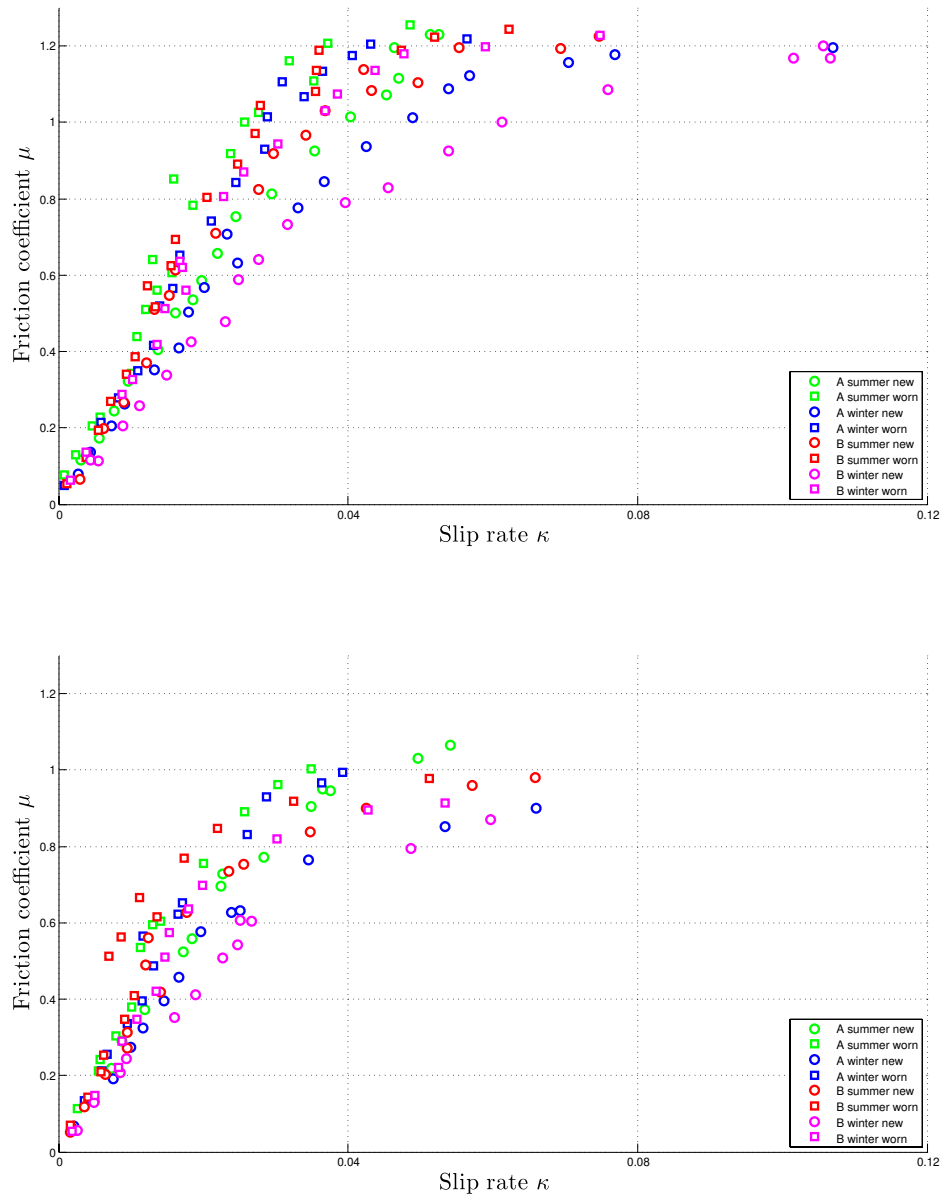


Figure 13. $\mu = f(\kappa)$ for Colgrip board (upper subfigure) and BBSG board(lower subfigure).

board cannot be represented because high grip cannot be reached on this pavement.

Observation of maximum friction coefficient values μ_{max} of figures 13 and 14 provides the ranking of tires according to their grip for a given pavement. For all pavements, except the Colgrip board which improves the poor performance of worn tires, the same ranking is observed :

- 1st : New summer tires.
- 2nd : New winter tires.
- 3rd : Worn summer tires.
- 4th : Worn winter tires.

This ranking is in accordance with our knowledge of tire characteristics.

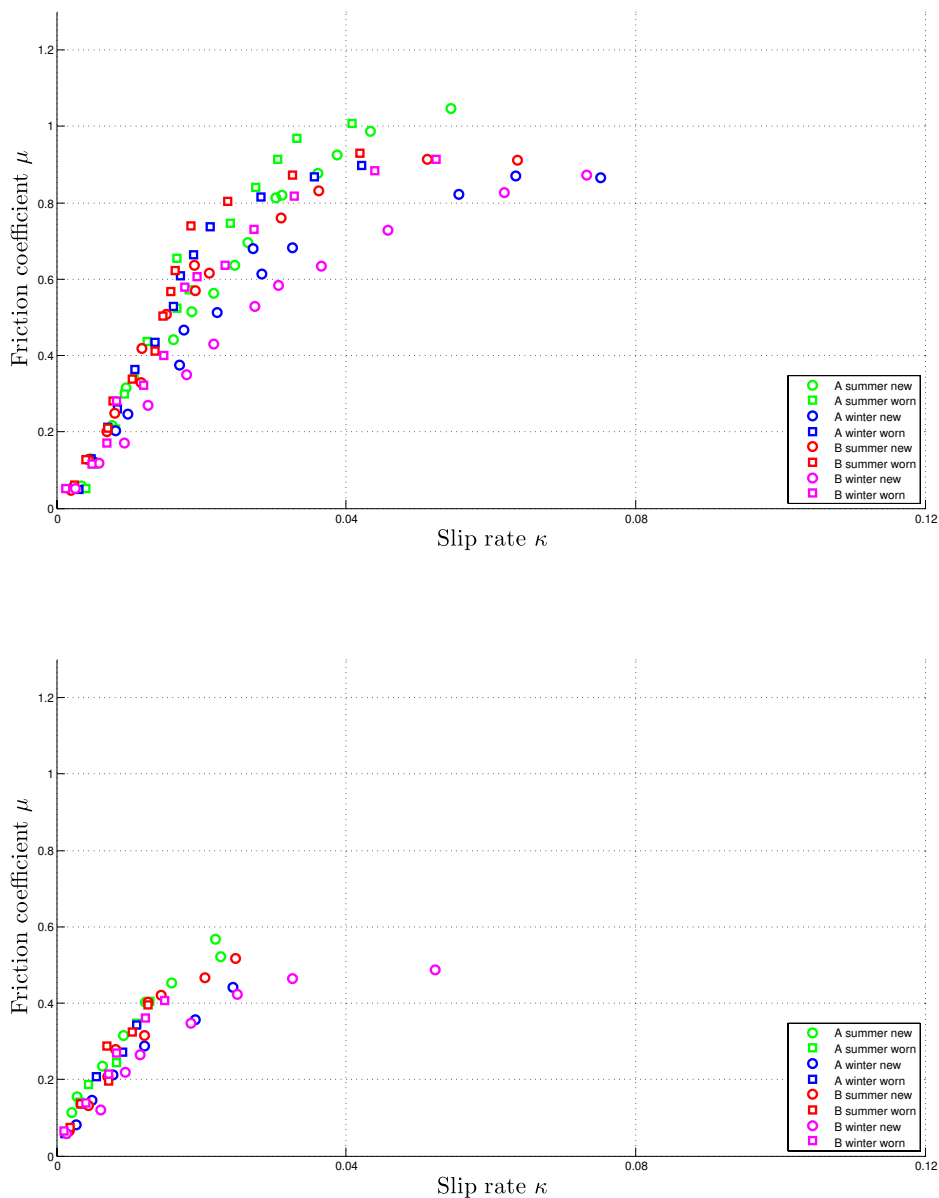


Figure 14. $\mu = f(\kappa)$ for Porous board (upper subfigure) and Painted board (lower subfigure).

Let us take into account the water thickness which is 0.4 mm on a traditional pavement. For this thickness, new tires are slightly more effective in draining water than worn tires. This explains the advantage of new tires.

The winter tires are more efficient at draining water. The high notch rate of the tire tread of winter tires implies a smaller gum surface in contact with the pavement than for summer tires. Consequently, winter tires are less efficient in dry conditions than summer tires. The quantity of water used in our experiments is not sufficient to show that their ability in draining water compensates their weakness in dry conditions. This explains the slight advantage of summer tires.

This ‘tire effect’ is emphasized on poor surfaces. On figures 13 and 14, the maximum available grip for the Painted board varies from $\mu_{max} = 0.35$ for a *A* worn winter tire to $\mu_{max} = 0.55$ for a *A* new summer tire. This difference in

friction can be explained by the difference in tread depth. A new summer tire has deeper tread than a worn winter tire (see table 3) so allowing it to drain more water.

The observation of tire/pavement longitudinal stiffness λ shows that the longitudinal stiffness of summer tires is greater than that of winter tires and the longitudinal stiffness of worn tires is greater than that of new tires for a given pavement. This observation is in accordance with our knowledge of tire characteristics. The gum trips of winter tires are smoother than those of summer tires in order to mould to the shape of road aggregates during bad weather. In addition the very small size of gum strips of worn tires increase their longitudinal stiffness.

4.4. Study of the slope variation of $\mu = f(\kappa)$ curves

This part presents a more detailed study of the variation of the longitudinal stiffness λ as a function of the maximum available grip μ_{max} . This study attempts to ascertain whether (or not) it is possible to estimate the maximum available friction coefficient μ_{max} from the longitudinal stiffness λ under normal driving conditions. In part 4.2, a doubt was expressed about this possibility. Figure 15 represents the longitudinal stiffness λ as a function of the maximum available friction coefficient μ_{max} , for all our test pavements and tires. For the sake of the clarity of the plot, μ_{max} values have been replaced by the board name. The Colgrip board presents $\mu_{max} = 1.24$, the BBSG board presents $\mu_{max} = 0.90$, the Porous board presents $\mu_{max} = 0.89$ and the Painted board presents $\mu_{max} = 0.4$. Results for the Epoxy board are not available because the regression cannot be performed on these data with a representative correlation coefficient.

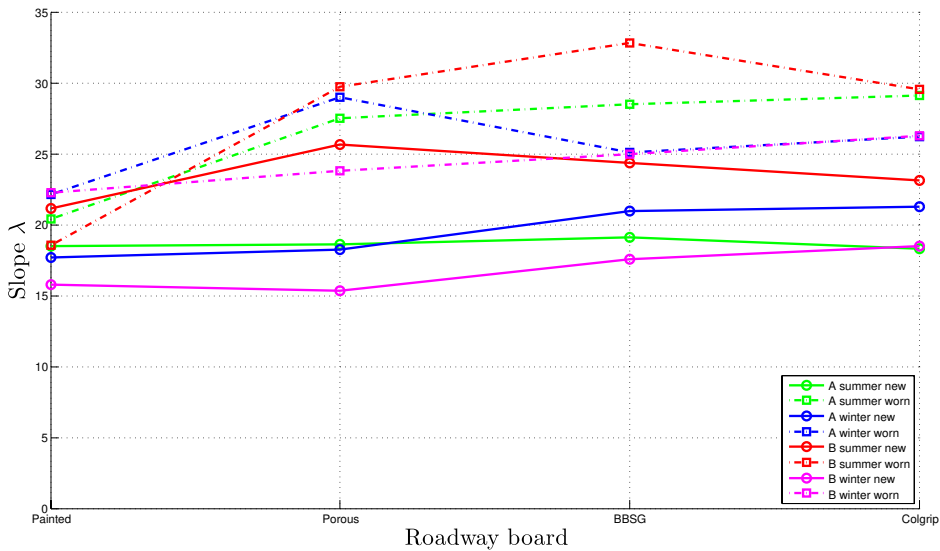


Figure 15. Longitudinal stiffness variation as a function of pavements.

Figure 15 shows that longitudinal stiffnesses obtained for the Painted board and for all tires are generally a bit lower than the others. The small amount of data measured on this board makes it a tricky calculation. Nevertheless, the values ob-

tained for λ using this board are close to the others and do not allow to distinguish it from other boards. Concerning the three other pavements, their longitudinal stiffness varies within the range $\lambda \in [15, 32]$ and present small differences. Consequently, their longitudinal stiffness λ does not allow discrimination between these four pavements, while their maximum friction coefficients vary from simple to triple and they present very different textures. Moreover, the results obtained show that it will be very challenging, maybe impossible, to estimate the maximum available grip μ_{max} from the longitudinal stiffness λ .

5. Discussion and conclusion

The purpose of this paper has been to present a measurement and a characterisation methodology for tire/pavement longitudinal friction. This work has been carried out to attempt to decide on the possibility, or not, on estimating the maximum available friction coefficient μ_{max} from the longitudinal stiffness λ for normal driving conditions. Moreover, this work has been motivated by the degree of importance of the knowledge of $\mu = f(\kappa)$ curves for models and applications described in the literature.

Due to the measurement difficulties, very few experimental works focus on the existence of the relationship $\mu_{max} = f(\lambda)$. This paper has presented experimental results. Using a trial vehicle equipped with a controlled deceleration system, $\mu = f(\kappa)$ curves have been obtained point by point on 5 different pavements and for 8 different tires. Test surfaces have been selected for their characteristics and representativeness of the French road national network. Different constant deceleration forces were applied to describe the totality of $\mu = f(\kappa)$ curves until ABS triggering and for a locked wheels braking. Using the proposed method, the high accuracy and repetitiveness of measurements have allowed us to study and to quantify the tire/pavement longitudinal stiffness and its variation as a function of the maximum available grip μ_{max} . The analysis of experimental data clearly show that there is no 'pavement effect'. In other words, a relationship $\mu_{max} = f(\lambda)$ does not exist.

This result is not in accordance with the literature. It questions the representativeness of some tire-road friction models and warns about the apparent simplicity of use of (5). Nevertheless from the pavement manufacturer point of view, experimental results show that a good pavement like Colgrip can improve tires performances. This observation opens a new investigation way for the design and the use of road in order to increase the controllability of future vehicles whatever the type or the weakness of their tires.

Moreover a new and efficient embedded method is proposed to tire/pavement characterisation. This method can be used as a complement to traditional tests using rolling machines or 'five wheels test vehicles' and presents the advantage of using real pavements with different texture scales with a real car.

This paper is also fruitful for road authorities for two reasons :

- Results increase the understanding of the influence of the road in the friction mechanisms. In particular, it will be useful to study the link between the conventional skid resistance (LFC), controlled by road authorities, and the skid resistance required by a real car.

- The procedure of controlled braking with a classical car opens new perspectives for measuring conventional skid resistance in area where the traditional 'five wheels test vehicles' cannot operate as in urban area.

Finally, we hope that the interest of the scientific community, which has invested much effort and time in tire/pavement friction estimation methods, will be renewed by these new results.

Acknowledgements

Authors thank P. Daburon, J.M. Prual and P. Bernier for their contribution in the realization of trials.

References

- [1] B. Breuer, U. Eichhorn, and J. Roth, *Measurement of tire road friction ahead of a car and inside the tyre*, in *AVEC'92 (International Symposium on Advanced Vehicle Control)*, Yokohama (Japan), 1992, pp. 347–353.
- [2] U. Eichhorn and J. Roth, *Prediction and monitoring of tyre road friction*, in *XXIV FISITA Congress*, June, , London (GB), 1992, pp. 2:67–74.
- [3] M. Khoudeir, J. Brochard, V. Legeay, and M.T. Do, *Roughness characterization through 3D textured image analysis: Contribution to the study of road wear level*, *Computer-Aided Civil and Infrastructure Engineering* 19 (2004), pp. 93 – 104.
- [4] A. Coiret, *Spectroscopic evaluation of pavement wetting states : Influence on wheel/ground friction*, *Bulletin des Laboratoires des Ponts et Chaussées* 255 (2005), pp. 137–155.
- [5] F. Gustafsson, *Slip-based tire-road friction estimation*, *Automatica* 33 (1997), pp. 1087 – 1099.
- [6] F. Braghin, M. Brusarosco, F. Cheli, A. Cigada, S. Manzoni, and F. Mancosu, *Measurement of contact forces and patch features by means of accelerometers fixed inside the tire to improve future car active control*, *Vehicle System Dynamics* 44 (2006), pp. 3 – 13.
- [7] F. Anfoso-Lédée and Y. Brosseau, *Rolling noise reduction from the road infrastructure: measurement methods and current practices*, in *4th International Congress on Automobile Comfort Acoustics and Vibrations* , *SIA-CTTM, Le Mans (France)*, November, , 2006.
- [8] H. Pacejka and E. Bakker, *Magic formula tyre model*, *Vehicle System Dynamics* 21 (1993), pp. 1 – 18.
- [9] M. Uchanski, *Road Friction Estimation for Automobiles Using Digital Signal Processing Methods*, University of California, Berkeley, 2001.
- [10] M. Burckhardt, *ABS und ASR, Sicherheitsrelevantes, Radschlupf-Regel Systeme* , University of Braunschweig, Germany, 1987.
- [11] C. Canudas-de-Wit, P. Tsiotras, E. Velenis, M. Basset, and G. Gissinger, *Dynamic friction models for road/tire longitudinal interaction*, *Vehicle System Dynamics* 39 (2003), pp. 189 – 226.
- [12] F. Gustafsson, *Slip-Based Estimation of Tire-Road Friction Estimation*, , Linköping University, Linköping, Sweden, 1993.
- [13] J. Gunnarsson, *Recursive Identification of Time Varying Parameters*, Linköping University, Göteborg, Sweden, 2001.
- [14] C. Lee, K. Hedrick, and K. Yi, *Real-time slip-based estimation of maximum tire-road friction coefficient*, *IEEE/ASME Transactions on mechatronics* 9 (2004), pp. 454–458.
- [15] Michelin, *Brevet FR2842910 Méthode d'asservissement, utilisable pour maintenir le glissement d'un pneu à niveau optimal pour qu'il fonctionne à un niveau de coefficient d'adhérence maximale*, , Société de Technologie Michelin, 2002.
- [16] P. Vandanjon, M. Do, Y. Delanne, A. Andrieux, and P. Daburon, *Comparison of different systems of measurement of skid resistance*, *Proceedings of the FISITA World Automotive Congress*, Yokohama, Japan (2006).
- [17] M. Gothié, *Use of piarc test tyres for the characterisation of skid resistance*, *RoutesRoads* 330 (2006), pp. 46–55.
- [18] Y. Delanne, *Skid resistance of tires: Conventional skid resistance, comparison and correlation with texture*, *Bulletin des Laboratoires des Ponts et Chaussees* (2005), pp. 35 – 49.
- [19] V. Cerezo and M. Gothié, *Adhera Research: A new approach for pavement performance evaluation*, *WEAR* 262 (2009), pp. 1105–1110.
- [20] W. Khalil and K. Hassan *Nonlinear systems - 3rd edition*, Upper Saddle River (New Jersey) : Prentice Hall, cop., 2002.
- [21] M.T. Do, P. Marsac, and A. Mosset, *Tribology Approach to predict the variation of Tire Wet Road Friction with Slip Speed*, in *Proceedings of the 5th International Symposium on Pavement Surface Characteristics*, Mai, , 2004, pp. 49–61.